

Bates College

SCARAB

All Faculty Scholarship

Departments and Programs

1-1-2022

Chemistry, Structure, and Function of Lone Pairs in Extended Solids

Geneva Laurita

Bates College, glaurita@bates.edu

Ram Seshadri

University of California, Santa Barbara

Follow this and additional works at: https://scarab.bates.edu/faculty_publications

Recommended Citation

Laurita, G. and Seshadri, R. (2022) Chemistry, Structure, and Function of Lone Pairs in Extended Solids. *Accounts of Chemical Research* 55 (7), 1004-1014. <https://doi.org/10.1021/acs.accounts.1c00741>.

This Article is brought to you for free and open access by the Departments and Programs at SCARAB. It has been accepted for inclusion in All Faculty Scholarship by an authorized administrator of SCARAB. For more information, please contact batesscarab@bates.edu.

Chemistry, Structure, and Function of Lone Pairs in Extended Solids

Geneva Laurita^{*,†} and Ram Seshadri^{*,‡}

†Department of Chemistry and Biochemistry

Bates College, Lewiston, Maine 04240, United States

‡Materials Department, Department of Chemistry and Biochemistry, and

Materials Research Laboratory

University of California, Santa Barbara, California 93106, United States

E-mail: glaurita@bates.edu; seshadri@mrl.ucsb.edu

Conspectus

The lone pair has been a known feature of the electronic structure of molecules for over one hundred years. Beginning with the pioneering work of Lewis and others that was later developed into useful guidelines for predicting molecular structure, lone pairs and their steric consequences are now taught at the very earliest stages of a chemistry education. In the crystalline solid state, lone pairs have perhaps had a less visible yet equally consequential role, with significant impact on a range of properties and functionality. Important properties associated with s^2 electron-derived lone pairs include their role in creating conditions favorable for ion transport, in the formation and correlation of local dipoles and the resulting polar behavior leading to ferroics and multiferroics, in increasing the refractive index of glass, in reducing the thermal conductivity of thermoelectric materials, and in breaking local symmetry permitting second harmonic light generation. In recent years, the role that the lone pair in developing the electronic structure of some topological quantum materials has also been recognized. While structural distortions due to lone pairs have traditionally been characterized through their crystallography, recent advances in scattering and spectroscopy have revealed the presence of local lone-pair driven distortions that do not correlate over long length scales. The role of these crystallographically “hidden” lone pairs, their detection, and their impact on properties has become a growing body of work in the literature. “Hidden” lone pairs are an effective argument for considering a role for lone pairs that goes beyond their being objects that occupy space in the coordination polyhedra of cations. This Account introduces the chemistry of lone pairs in extended crystalline solids, including a discussion of when they are stereochemically active, how they manifest in the structure, and how their chemistry can be tuned by the chemical environment around them. Eventually, all of these factors work in unison to help develop and tune properties of interest. Certain specific examples of structure-property relations in materials that are driven by lone pair behavior are described here, including the potential impact of lone pairs on the optical and electronic properties of hybrid halide perovskite compounds that are relevant to their photovoltaic applications. We

highlight the role of lone pairs in the dielectric behavior of geometrically frustrated pyrochlores, the temperature-dependent optoelectronic behavior of halide perovskites, the polar phase transitions in lead-free ferroelectric perovskites, and the compositional insulator-to-metal transition in ruthenium pyrochlores. The theme underpinning this account is that the lone pair can be considered as a powerful design element for a broad range of material function.

1 Key References

- Fabini, D. H.; Laurita, G.; Bechtel, J. S.; Stoumpos, C. C.; Evans, H. A.; Van der Ven, A.; Kanatzidis, M. G.; Seshadri, R. Dynamic Stereochemical Activity of the Sn²⁺ Lone pair in Perovskite CsSnBr₃. *J. Am. Chem. Soc.* **2016**, *138*, 11820–11832.¹ The role of crystallographically “hidden” lone pairs on the structure, dynamics, and optical properties of a prototypical halide perovskite of Sn²⁺ is revealed through monitoring the temperature-dependence of the average and local structure and the photoluminescence, coupled with density functional theory (DFT)-based electronic structure modeling.
- Laurita, G.; Fabini, D. H.; Stoumpos, C. C.; Kanatzidis, M. G.; Seshadri, R. Chemical Tuning of Dynamic Cation Off-Centering in the Cubic Phases of Hybrid Tin and Lead Halide Perovskites. *Chem. Sci.* **2017**, *8*, 5628–5635.² The local and crystallographic behavior of lone pairs as a function of chemistry in a series of hybrid halide perovskites is described through the analysis of synchrotron X-ray total scattering data.
- Laurita, G.; Page, K.; Suzuki, S.; Seshadri, R. Average and Local Structure of the Pb-Free Ferroelectric Perovskites (Sr,Sn)TiO₃ and (Ba,Ca,Sn)TiO₃. *Phys. Rev. B.* **2015**, *92*, 214209.³ The role of lone pair chemistry on the ferroelectric behavior of Sn²⁺-substituted perovskite oxides is examined through neutron total scattering studies.
- Laurita, G.; Puggioni, D.; Hickox-Young, D.; Gaultois, M. W.; Lamontagne, L.; Page, K.; Rondinelli, J.; Seshadri, R. Uncorrelated Bi Off-Centering and the Insulator-to-Metal Transition in Ruthenium A₂Ru₂O₇ Pyrochlores. *Phys. Rev. Mater.* **2019**, *3*, 095003.⁴ The influence of disordered lone pairs on the observed compositionally-driven insulator-to-Metal transition in the pyrochlore Pr_{2-x}Bi_xRu₂O₇ solid solution is presented, through a combination of neutron total scattering analysis and DFT-based electronic structure modeling.

2 Introduction

Negative corpuscles — soon to become better known as electrons — were discovered in cathode rays by J. J. Thomson in 1897.⁵ It did not take much longer for several researchers, including Lewis,⁶ to recognize the preeminent role that electrons, or more precisely, pairs of electrons play in the chemical bond (a fascinating early history, including controversies surrounding priority has been presented by Jensen⁷). Lone pairs are the pairs of electrons in Lewis theory that are not shared between atoms. In the structural chemistry of main group elements, lone pairs are ubiquitous and familiar. In the first half of the 20th century, advances in crystallography and improved familiarity with electron counting led to the familiar valence shell electron pair repulsion (VSEPR) theory of Sidgwick and Powell⁸ and improved upon by Gillespie and Nyholm.⁹ VSEPR theory introduces the role of the bonding pairs and lone pairs as they pertain to the geometry of molecules of main group elements. In covalent molecules in the solid state, the presence of lone pairs is readily revealed through the shape of the molecule and through, for example, patterns of hydrogen bonding when it exists.

In figure 1a, the crystal structures (all structure depictions created with the VESTA software suite¹⁰) of heavy, D₂O ice-VIII is presented, as obtained from a neutron study¹¹ that was carried out at a temperature of 10 K and under a 2.4 GPa pressure. This structure was chosen because it does not display the proton/deuteron disorder issue found across several phases of ice. Besides the two covalently bonded deuterons, the two lone pairs on each oxygen form secondary bonds (depicted with dashed lines) with deuterons on neighboring D₂O molecules. Were it not for the lone pairs on the oxygen in water, water would not have a dipole moment or be able to hydrogen bond, and would therefore behave very differently; of great consequence to all life processes (see, for example, the collection of articles in¹²). Figure 1b displays the crystal structure of ND₃ determined at a temperature of 2 K from neutron diffraction.¹³ The familiar geometry of the ammonia molecule arises once again from the lone pair of electrons on nitrogen. The ammonia molecule famously

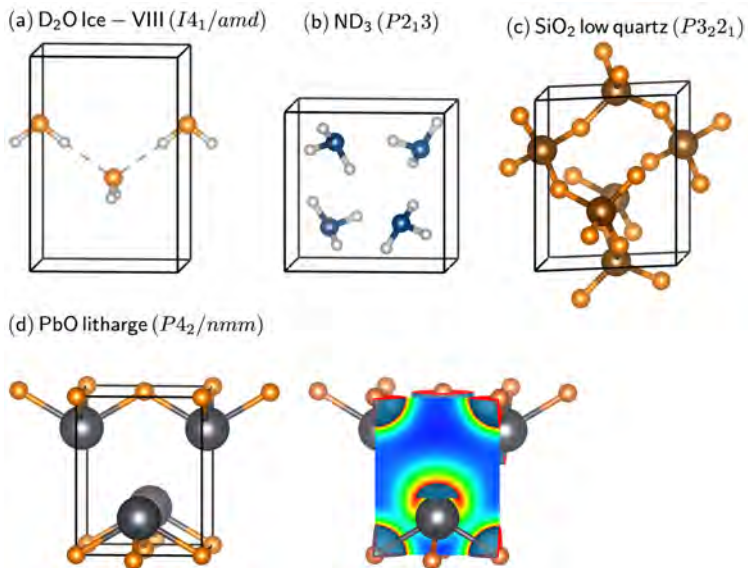


Figure 1: Solid state crystal structures from neutron and X-ray measurements of (a) D_2O molecules in ice-VIII at 10 K and 2.4 GPa (only a few molecules are displayed in the unit cell, for clarity), (b) the low-temperature crystal structure of heavy ammonia ND_3 at 2 K, (c) the low-quartz crystal structure of SiO_2 and the (d) crystal structure of α -PbO. At the right is a depiction of the same structure with the electron density associated with the lone pair lobe on Pb^{2+} displayed for an isosurface value of $0.17 e^- \text{ \AA}^{-3}$.

inverts like an umbrella in the gas phase, with a corresponding strong absorption in the microwave region of the electromagnetic spectrum as a consequence of the dipolar character of the transition. It is this absorption that allowed the construction of the first ammonia maser.¹⁴

In SiO_2 (the low-quartz crystal structure¹⁵ displayed in figure 1c), similarly to the structure of water, the lone pairs on oxygen result in all of the Si–O–Si bond angles deviating quite significantly from an angle of 180° to something closer to 144° . Finally, figure 1d displays the crystal structure of litharge, which is the α form of PbO. If the Pb^{2+} ion were to behave like a typical divalent cation, for example Sr^{2+} which it resembles in terms of radius, the expected crystal structure would be a rock-salt. Instead, an unusual tetrapodal coordination for Pb^{2+} is observed that allows every lone pair on Pb^{2+} to express itself in the crystallography of this compound, forming a layered structure with the lone pairs between sheets of Pb^{2+} ions.

Notwithstanding structures such as those of α -PbO being familiar now for nearly a century, it would be accurate to say that in the extended solid state, understanding the role of lone pairs as they relate to structure and bonding has been more recent. The work was largely initiated by Orgel,¹⁶ with more recent contributions from several others, summarized in reviews by Walsh¹⁷ and Bersuker.¹⁸

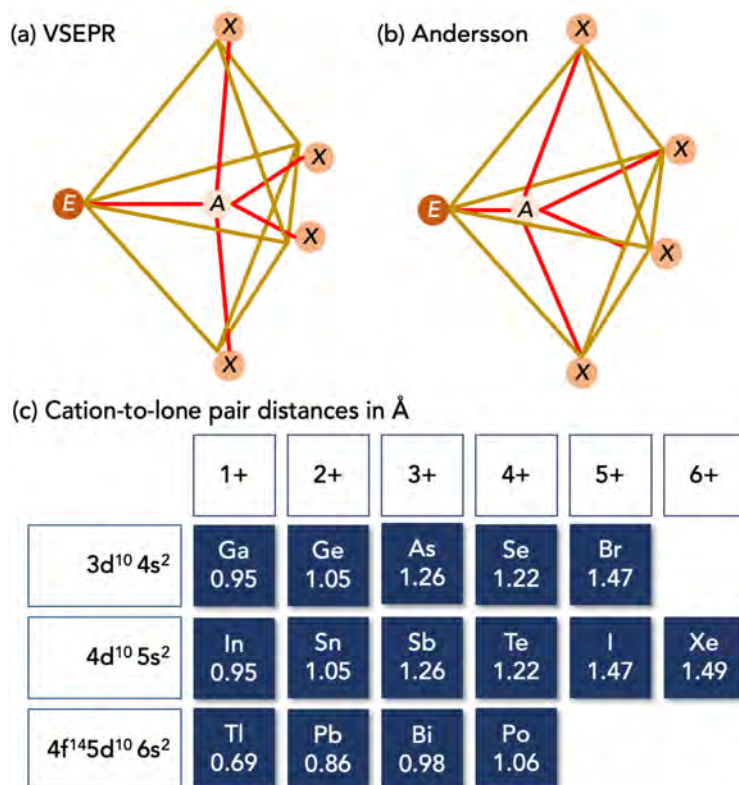


Figure 2: (a) VSEPR prediction for the coordination geometry of a AX_4E polyhedron, displaying the consequences of the lone-pair E being more repulsive than $A-X$ bonds. (b) The correction by Andersson suggesting that the principle distortion of the coordination polyhedron is due to the off-centering of the cation as a consequence of the shortened $A-E$ distance. (c) Typical, empirically obtained cation-to-lone pair distances for the main group cations that display an oxidation state that is 2 less than the group oxidation state, and that each have a single ns^2 -derived lone pair.

A crystallography-driven approach motivated Sten Andersson and coworkers^{19,20} to slightly tweak the VSEPR rules to properly account for the surprisingly large volume of the lone pair, allowing better prediction of the geometry of coordination polyhedra. Their detailed analysis of lone-pair containing crystal structures allowed the development of design

principles that have been summarized in the well-regarded book of Hyde and Andersson.²¹ The summarized data include typical central atom-to-lone pair distances, and the idea that the lone pair typically takes up the same volume as an oxide or fluoride anion in the space of the coordination polyhedron. The Andersson model has not been widely disseminated, and it is appropriate to reproduce the gist of it, here in figure 2. Panel (a) and (b) of this figure compare the VSEPR and Andersson predictions of the geometry of a AX_4E coordination polyhedron where X are oxide or fluoride anions around a central cation A that has a single lone pair E .²² Either model suggests that a single set of lone pairs in the central cation should perforce create a local dipole, provided the lone pair displays stereochemical activity, which as we shall see presently, is not always the case.

The Andersson model²² suggests that the cation-to-lone pair distance is significantly smaller than cation-anion distances, while the volume of the lone pair is similar to the volume of the oxide or fluoride anion. Panel (c) of this figure reproduced the empirically obtained distances presented in the book of Hyde and Andersson.²¹ The trends in the cation-to-lone pair distances do not follow an intuitive pattern. From the table of distances seen in figure 2(c), it is seen that higher charges on the cation, and smaller cations have larger distances to the lone pair. The trends on going from $4s^2$ and $5s^2$ to $6s^2$ are also sudden, and these arise due to a combination of the lanthanide contraction and scalar-relativistic effects, manifesting in the so-called inert-pair effect.²³

The widespread adoption of increasingly reliable density functional theory (DFT)-based electronic structure calculations for extended, crystalline solids,^{24,25} and the development of a variety of ways to depict features of bonding, including through the use of the electron localization function (ELF)^{26,27} has contributed greatly to a better understanding of structure and function in solids containing lone-pair ions.²⁸

In this Account, we describe some of the more fascinating aspects of lone pair behavior in the solid state, biased by our own research in the area. We start by considering the chemistry of the lone pair, including the times when it does not appear to impact the

crystal structure, and then go on to aspects of structure and function. There are several aspects of lone pair behavior not considered in this account. A partial list includes their role in ion conducting materials,²⁹ in phase change materials,³⁰ their ability to reduce thermal transport in thermoelectrics,^{31–33} band structure inversion in semiconductors such as GeTe, SnTe, and PbTe³⁴ more recently associated with topological properties in materials like SnTe,^{35,36} and finally, their use as a symmetry-breaking element in non-linear optical materials.^{37,38}

3 Chemistry and Stereochemical Activity

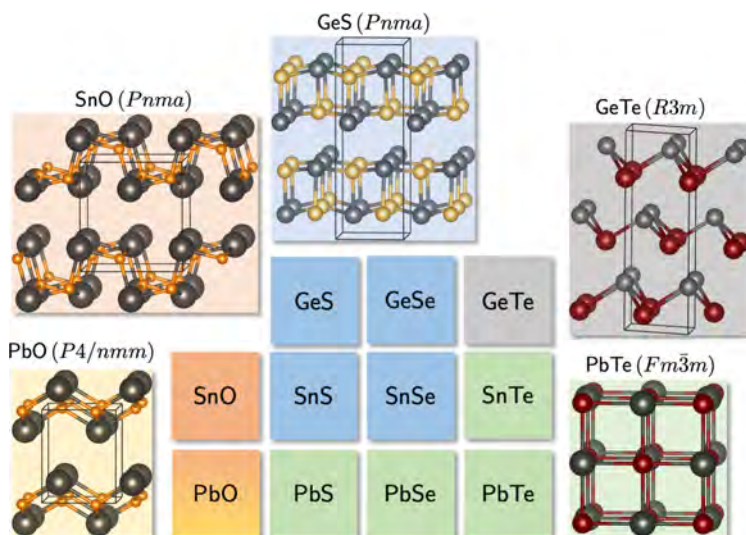


Figure 3: Room-temperature crystal structures of oxides and chalcogenides of the divalent tetrel (carbon group) elements. In some of the crystal structures, lone pairs manifest clearly, *ie.* are stereochemically active, while in others, notably those with rock salt structures (in space group $Fm\bar{3}m$), the lone pair is hidden.

When cations with lone pairs are found in crystal structures where the lone pair manifests itself in some obvious structural manner, for example through the creation of distorted polyhedra around the cation, the lone pairs are described as being stereochemically active. From the viewpoint of crystallography, such distortions are observed when they are coherent and correlated over a long range. However, it is frequently the case that lone-pair

bearing cations are also found in structures where the cations are in highly symmetrical environments. This is well-illustrated by the oxides and chalcogenides of the tetrel (carbon group) elements as illustrated in figure 3. If the lone pair had purely s^2 character and were spherically symmetric, then all lone-pair bearing compounds would be expected to be stereochemically silent, rather than active. It was Orgel who first suggested that there must be some s and p mixing (that he felt took place on the cation, *ie.* hybridization) that allows the lone pair to be stereochemically active.¹⁶ However, considering figure 3, it is clear that the nature of the anion plays a decisive role, and anion states must be implicated, *ie.* covalency has a role to play, as has been pointed out by several investigators.^{39–43} In the molecular world, the role of anion electronegativity in dictating the orbital character of the lone pair has been long established.⁴⁴ The role of π bonding and the size of the central cation in modulating lone-pair activity in molecules is also well known.⁴⁵

Waghmare *et al.*⁴⁶ considered the electronic structural reasons for lone-pair activity (or absence thereof) associated with the tetrel sulfides, selenides, and tellurides using first-principles electronic structure calculations and established that it is the stereochemical activity of the cation lone pair which drives structural deviations from regular cation-anion octahedra in all of these materials, determined by the interaction of cation s and p states with anion p states. Additionally the nature of the phonon spectra calculated for the cubic rock salts of the nine compounds — specifically the extent of the energy splitting between the longitudinal and transverse optical phonons (LO-TO splitting) — anticipates the nature of the true ground state structure.

A clear and accessible explanation of the origins of ns^2 -derived lone pair behavior has been presented in the recent text by Woodward *et al.*⁴⁷ on the basis of second order Jahn-Teller distortions. Unlike the more familiar first-order Jahn-Teller distortion, which is associated with symmetry lowering in order to lift a degeneracy, in the case of lone-pair induced distortions, all states are either filled or empty and the distortion is driven by the stabilization of a filled state, by adding some bonding character to a non-bonding state.

This is most simply illustrated by considering the NH_3 molecule. A planar NH_3 molecule would involve a completely non-bonding and filled p_z orbital on N. The distortion to the familiar pyramidal geometry permits some mixing of the p_z orbital with the empty N $2s - \text{H } \sigma^*$ molecular orbital, permitting slight stabilization.

In those binary chalcogenides with distorted environments, the local distortions of polyhedra are correlated over long length scales permitting their observation using average crystallographic techniques such as Bragg diffraction. However, if the local environment were to be distorted but in an incoherent, uncorrelated manner (for example, with the direction of the cation off-centering varying in different and random directions) this will result in an average of the positions, and in the crystallographic structure the cation appears to be located in the center of the coordination environment. Therefore, the structure determined from diffraction is an inaccurate representation of the symmetry around the cation, obscuring the existence of dipoles, as well as leading to inaccurate conclusions about the bonding and orbital overlap of the atoms in the material. A striking example of this is the reported “emphanisis” in SnTe, PbS, PbTe.^{48,49} It was observed through local pair distribution function (PDF) analysis that an incoherent, distorted Sn/Pb environment emerged upon warming while the average structure remains crystallographically cubic, proposed to be due to a crossover between an lone-pair inactive and lone-pair active state as a function of lattice expansion. Therefore, in order to have a complete view of the structure-property relationships in a material, one must take a holistic view of the material through an analysis of both the crystallographic (meaning average symmetry) and local coordination environments present.

When lone pair stereochemical activity is uncorrelated, it can be reflected in Bragg crystallographic analysis as enlarged atomic displacement parameters or as split atoms in reduced symmetry crystallographic sites. While this hints at an underlying structural distortion on the local scale, the nature of this disorder can be varied. For example, a material may exhibit static disorder, where in the case of lone pair stereochemical ac-

tivity the cations are off-centered in a random direction. In this case, the off-centering magnitude is consistent and the local dipole is fixed, but the material lacks long-range ordering of dipoles. Alternatively, a material may display dynamic disorder in which the local dipoles fluctuate in either magnitude or direction, which hinders long-range ordering and the presence of a crystallographically distorted phase. Typically the two types of disorder can be distinguished by temperature-dependent studies, where dynamic disorder dominates at higher temperatures, while static disorder persists upon cooling. The use of complementary spectroscopic techniques, or quasielastic scattering techniques such as the dynamic pair distribution function⁵⁰ that are simultaneously sensitive to spatial and temporal correlations can provide insights into the precise nature of the disorder.

One example of local disorder due to lone pairs is the “charge ice” atomic displacement of cations in the pyrochlore $\text{Bi}_2\text{Ti}_2\text{O}_7$, illustrated in figure 4a.⁵¹ $\text{Bi}_2\text{Ti}_2\text{O}_7$ is chemically analogous to the prototypical ferroelectric perovskite PbTiO_3 , containing both a s^2 and d^0 cation. However, when lone pair cations are present on the pyrochlore lattice, there is a tendency for site disorder to stabilize the structure.^{54–57} This results in off-centering of the lone pair-active cation in an incoherent, frustrated fashion due to geometric considerations of the cation arrangement. In PbTiO_3 , the octahedra are corner-shared in such a way that the cations form a square lattice, and off-centering can be correlated so that a polar structure is realized. While the octahedra are still corner-shared in the pyrochlore lattice, the arrangement is such that the cations form a three dimensional triangular lattice. Analogous to frustrated magnetic spins on a kagome lattice,⁵⁸ cation off-centering is frustrated in the pyrochlore structure, resulting in what we refer to as a “charge-ice” arrangement at lower temperatures instead of a coherent, polar phase.⁵¹ This manifests crystallographically as enlarged, flat displacement ellipsoids on the Bi^{3+} site (figure 4a), which can be further resolved by a split site model with the Bi cations displaced from their ideal $16d$ central site and the lone pair density is smeared in a ring around the site, illustrated in figure 4b and c. This additionally results in disorder on the O' site (figure 4d),

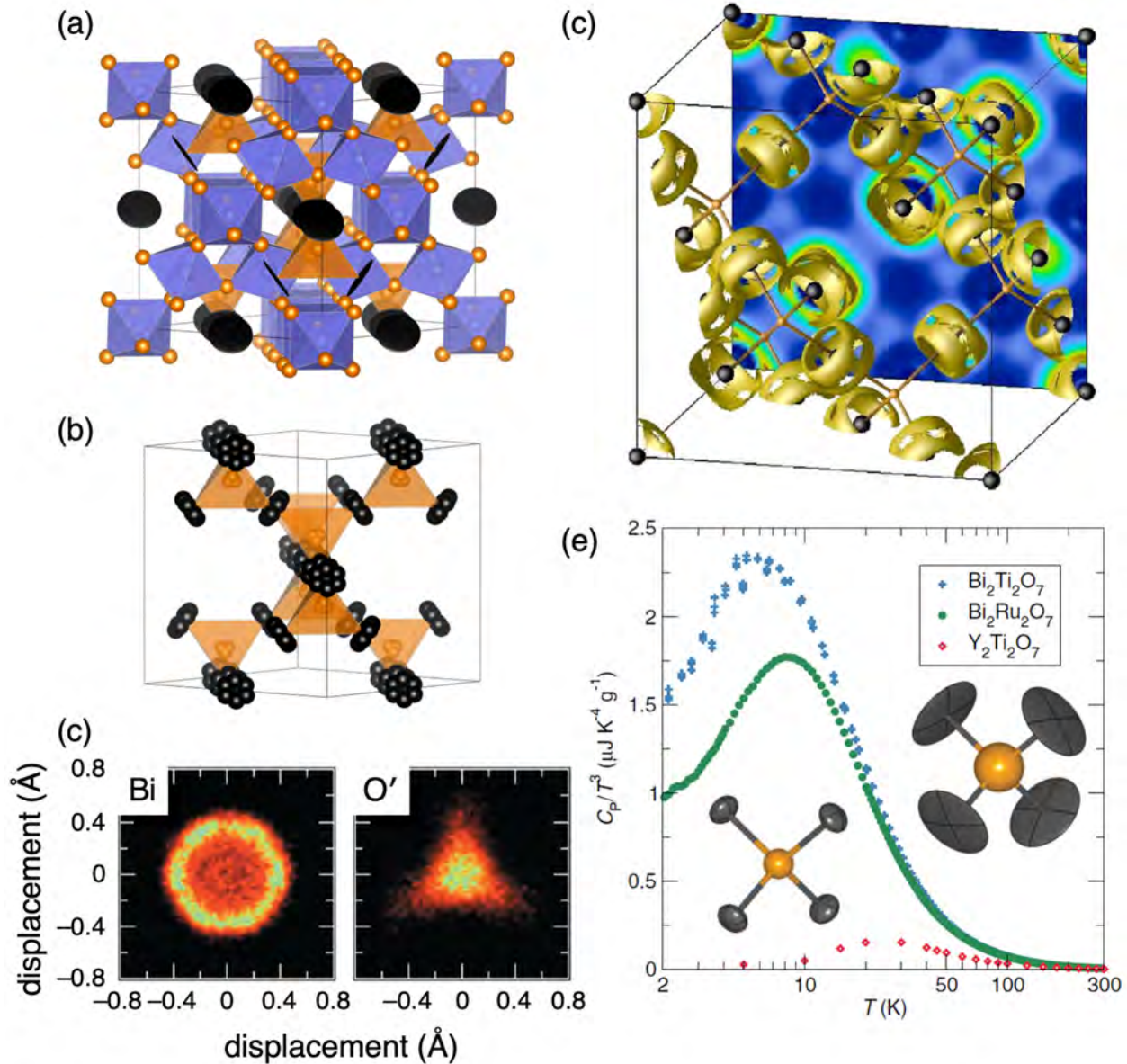


Figure 4: The $\text{Bi}_2\text{Ti}_2\text{O}_6\text{O}'$ crystal structure is shown in (a) with 50% thermal ellipsoids representing the atomic displacement parameters from Rietveld refinement at 14 K. The two interpenetrating networks are of corner-sharing TiO_6 octahedra (blue) and corner-sharing $\text{O}'\text{Bi}_4$ tetrahedra (orange). Disorder of Bi (grey disks) can be modeled using six-fold split Bi and four-fold split O' , network shown in (b). (c) Bi– O' network of $\text{Bi}_2\text{Ti}_2\text{O}_6\text{O}'$ showing the valence electron localization isosurfaces visualized for a value of $\text{ELF} = 0.65$. The total ELF for a single plane is projected on the back of the unit cell. The localization scale runs from deep blue ($\text{ELF} = 0$) to white ($\text{ELF} = 1$). (d) Atomic positions for Bi and O' at 14 K from 14 independent RMC simulations. (e) Heat capacities of three pyrochlores show a strong dependence on the magnitude of static A-site disorder (large in $\text{Bi}_2\text{Ti}_2\text{O}_6\text{O}'$, present in $\text{Bi}_2\text{Ru}_2\text{O}_6\text{O}'$, and none in $\text{Y}_2\text{Ti}_2\text{O}_7$). Adapted with permission from ref. ⁵¹ (Copyright 2006 Elsevier Masson SAS) ref. ⁵² (Copyright 2010 American Physical Society) and ref. ⁵³ (Copyright 2011 American Physical Society).

which can also be captured in a split-site crystallographic model.⁵² The success of using a split-site model suggests this disorder is static in nature, and this is further evidenced by temperature-dependent heat capacity measurements (figure 4e) on a series of $A_2B_2O_7$ pyrochlores: when A is the lone-pair bearing Bi^{3+} , the heat capacity of the material increases upon cooling, whereas this behavior is not observed when $A=\text{Y}^{3+}$, which has an s^0 electronic configuration.⁵³ While this disordered behavior is desirable for high dielectric constant materials,⁵⁹ the lack of correlated displacements prevents piezo- or ferroelectric behavior.

Our work has identified the effect of lone-pair induced dynamic disorder in the halide perovskite CsSnBr_3 , an inorganic analog of the heavily studied organic-inorganic hybrid halide perovskites.¹ Comparing the temperature dependent X-ray PDFs between 300 K and 420 K revealed the evolution of peak asymmetry in the Sn—Br bond upon warming (figure 5a) while the structure remained crystallographically cubic, similar to the effect of “emphanisis” identified in the binary chalcogenides. Through refinement of the PDF in this temperature regime, it was determined that the peak asymmetry was best modeled by the rhombohedral $R3m$ perovskite structure in which the Sn^{2+} is displaced along the [111] direction towards the face of the SnBr_6 octahedra, with the lone pair localizing opposite the cation displacement (figure 5b and c). This observation was further corroborated by DFT-based electronic structure calculations, which indicated the development of a minimum in the energy landscape off the nominal crystallographic position upon lattice expansion in lone-pair bearing cations Sn^{2+} and Pb^{2+} , while the nominal crystallographic position remains the minimum when no lone pair is present in CsCaBr_3 . This energy landscape exhibits a highly anharmonic shape when lone-pairs are present, which is proposed to play a role in several of the important properties that make these materials promising candidates for photovoltaic applications.

We have additionally observed this temperature-activated, dynamic displacement of the lone-pair bearing cation across a series of halide perovskites AMX_3 (where $A^+ = \text{CH}_3\text{NH}_3$

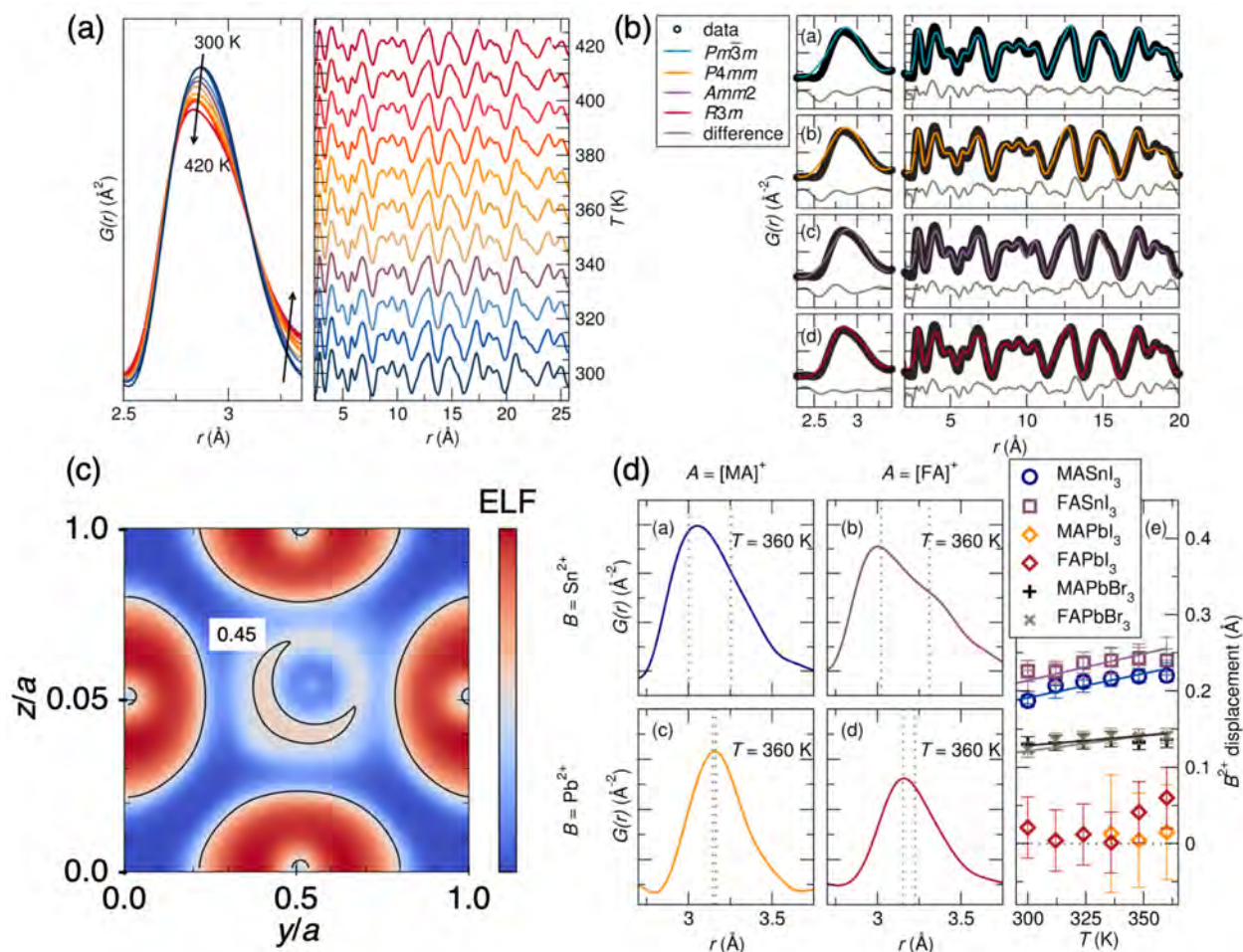


Figure 5: Temperature-driven, dynamic stereochemical activity of Sn²⁺ lone pairs in CsSnBr₃ evidenced by (a) an evolution in the peak asymmetry of the Sn-Br peak in temperature dependent XPDF data (11-ID-B, Argonne National Laboratory) upon warming. (b) Various models of Sn²⁺ displacement indicate the best fit is obtained with the off-centered $R3m$ model. (c) The electron localization function (ELF) of CsSnBr₃ on a (200) slice of the unit cell (a plane through the nominal Sn site), with Sn²⁺ displaced 0.4 Å, along [111] and $\Delta a = 5\%$, (d) $M-X$ peak in the XPDF (11-ID-B, Argonne National Laboratory) of a series of AMX_3 hybrid perovskites illustrate the largest off-centering when $A = FA^+$, $M = Sn^{2+}$, and $X = Br^-$. Adapted with permission from ref. ¹ (Copyright 2016 American Chemical Society) and ref. ² (Copyright 2017 Royal Society of Chemistry).

(MA) or $\text{CH}(\text{NH}_2)_2$ (FA); $M^{2+} = \text{Sn}$ or Pb ; $X^- = \text{Br}$ or I).² The magnitude of the displacement follows that of the predicted chemical trends that dictate stereochemical activity: the larger *A*-site cation FA^+ , the smaller *M*-site cation Sn^{2+} , and the harder *X* anion Br^- promotes the largest off-centering of the central cation (figure 5d). From these results, it is predicted that this thermally-activated lattice instability may also be present in similar hybrid perovskites and may further be a wide-spread local phenomena present in a range of material systems. In addition to the fundamental interest, we illustrated that this phenomenon affects the temperature dependence of the observed photoluminescence of CsSnBr_3 (discussed further in Function), and is proposed to have optical and electrical impacts due to the deformability and polarizability of the lattice.

4 Function

Cooperative and long-range lone pair effects play a critical role in determining the properties of many materials, particularly in regards to the interaction with light and electric fields. Cooperative distortions that result in a non-centrosymmetric structure lead to a wealth of technologically relevant functional properties, including second harmonic generation, piezoelectricity, pyroelectricity, and ferroelectricity. Ferroelectrics are a class of electrically insulating, or dielectric, materials that exhibit a spontaneous electrical polarization that is switchable in the presence of an external electric field. They support a variety of technological applications including capacitors, actuators and transducers, sonar, and medical imaging.

Many polar solid state materials have perovskite or perovskite-derived structure types, with the cubic aristotype having the chemical formula ABX_3 , in which the larger *A*-site cation is coordinated to 12 anions in a cuboctahedral environment, while the smaller *B*-site cation is octahedrally coordinated to the *X* anions (figure 6a). The ratio of the size of the *A* and *B*-site cations, determined through the Goldschmidt tolerance factor,⁶⁰ dic-

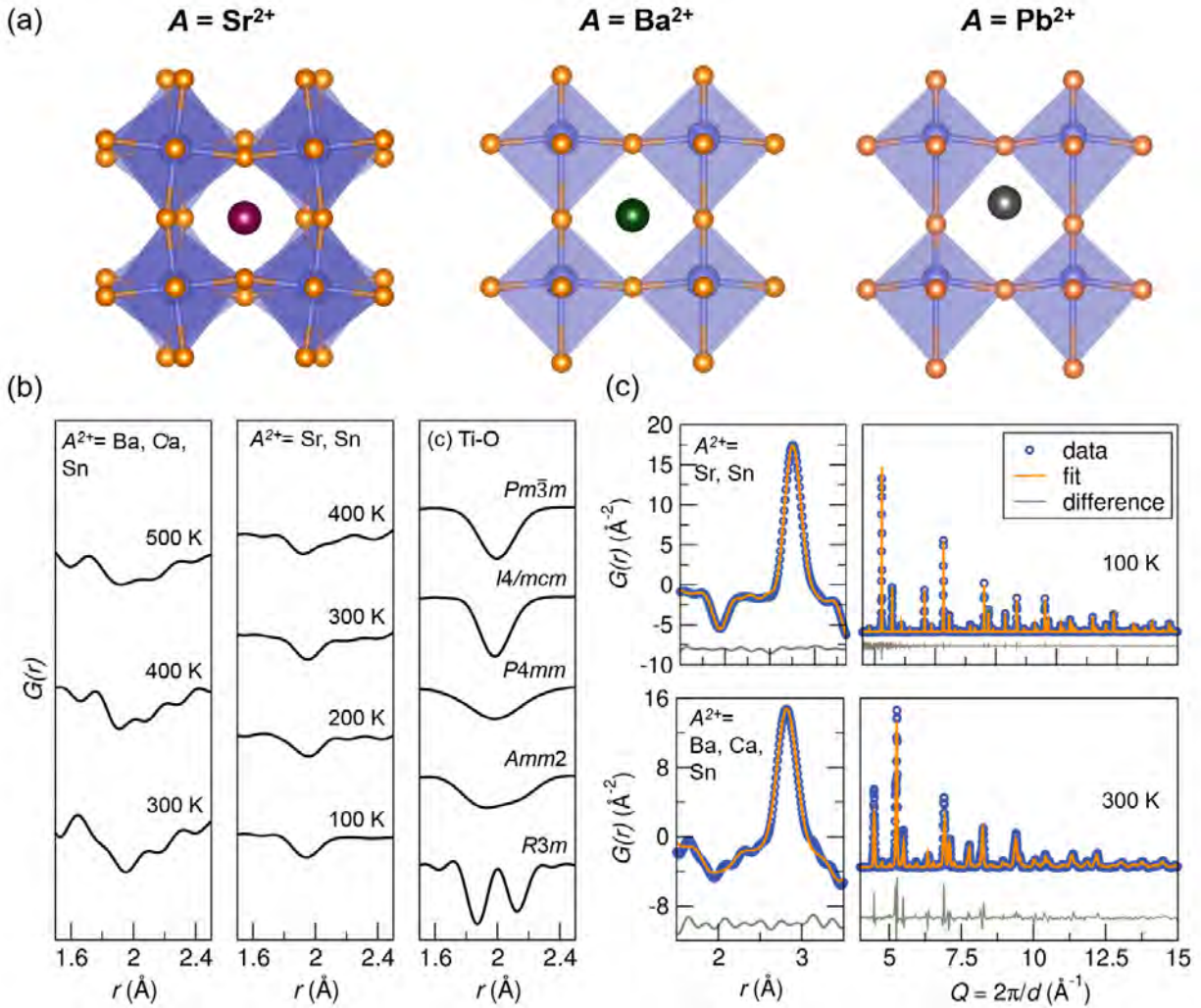


Figure 6: (a) Structural distortions observed upon cooling in prototypical perovskites SrTiO₃ (*I4/mcm*), BaTiO₃ (*R3m*), and PbTiO₃ (*P4mm*). (b) Evolution of the Ti-O peak in neutron PDF (NOMAD, Oak Ridge National Laboratory) data when a small amount of lone-pair bearing Sn²⁺ is substituted into (Ba,Ca)TiO₃ and SrTiO₃. (c) Substitution of Sn²⁺ alters the low-symmetry structures of the parent compounds, and both the PDF and diffraction data (NOMAD, Oak Ridge National Laboratory) of both samples is best described by the *P4mm* adopted by PbTiO₃. Adapted with permission from ref³ Copyright 2015 American Physical Society.

tates the structural behavior of the perovskite. In SrTiO_3 , the cubic perovskite undergoes a phase transition in which the TiO_6 rotate to accommodate the smaller Sr^{2+} cation, resulting in the non-polar, centrosymmetric $I4/mcm$ phase. If A is a larger cation such as in BaTiO_3 , the Ti–O bonds in the TiO_6 octahedra elongate to accommodate the larger cation, and there is a subsequent off-centering of the Ti. This results in a non-centrosymmetric, polar phase. In PbTiO_3 , the $6s^2$ -derived lone pair of electrons associated with the Pb^{2+} readily hybridizes with the $2p$ orbitals of the neighboring oxygen. The result is a cooperative distortion of both the Pb–O polyhedral environment and the TiO_6 octahedra below a critical temperature, T_c . These collective distortions result in a long-range, polar crystal structure that is symmetrically described by the space group $P4mm$ and below T_c the material exhibits ferroelectric behavior. Due to the cooperative distortions of both the Pb and Ti environments, the observed spontaneous polarization is large and the T_c occurs above room temperature, both desirable for ferroelectric applications. However, the toxic nature of Pb prompts the search for a Pb-free alternative to increase the applicability of perovskite ferroelectrics.

In Pb-based piezo- and ferroelectric materials, each Pb^{2+} cation has a lone pair of electrons that contributes to a long range distortion of the crystal structure. However, our work at Oak Ridge National Laboratory (figure 6b, c) demonstrated that even a small substitution of Sn^{2+} , a smaller congener of Pb^{2+} , into SrTiO_3 (approximately 10 %) can induce ferroelectric behavior, and it was observed through the neutron PDF that local polar nano-regions are present even at room temperature. This work also revealed that the presence of Sn^{2+} into $(\text{Ba,Ca})\text{TiO}_3$ (approximately 5 %) alters the nature of the phase transitions and local polar regions. This work revealed that the Sn^{2+} lone pair drives the material to mimic the phase transitions of PbTiO_3 rather than unsubstituted SrTiO_3 or $(\text{Ba,Ca})\text{TiO}_3$. Thus, our initial results support the viability of this Pb-free material for ferroelectric applications. In addition to crystallographic structural transitions, the $6s^2$ -derived lone pair of electrons played a surprising role in the nature of the symmetry of the TiO_6 octahedra. We

observed through neutron PDF that the local Ti environment became more regular upon cooling, contrary to typical behavior, where transitions to lower symmetry are generally observed with decreasing temperature (figure 6b). This work illustrated the importance of even a small number of lone pair of electrons on both the short-range ordering and long-range structural transitions.

When combined with a magnetic ion, lone pair stereochemical activity can contribute to multiferroic behavior, where there is a simultaneous long-range ordering of electric and magnetic dipoles. Lone-pair containing ABO_3 perovskites have particularly been closely examined in this regard since they permit a separation of the lone pair containing ion on the A site from the magnetic ion on the B site.^{28,61,62}

Lone-pair driven structural changes influence functionality beyond the formation of local or correlated electrical dipoles. Any structural distortion will alter the bond lengths and bond angles between the constituent atoms, and this directly influences the degree and nature of orbital overlap. This can be observed in the optical properties of a material through the evolution of the band gap as a function of temperature. While it is expected that bond lengths will increase with temperature-induced lattice expansion, thus weakening orbital overlap, deviations from expected behavior can hint at structural distortions in play. For example, our work on the dynamic off-centering in the $CsSnBr_3$ illustrated this in the photoluminescent (PL) behavior as a function of temperature.¹ $CsSnBr_3$ has a phase transition at 286 K between a tetragonal and cubic phase (figure 7a), and both phases exhibit large unit cell expansions upon warming (121 ppm K^{-1} and 108 ppm K^{-1} , respectively) and a blue shift of the PL emission peak energy (figure 7b). While the expansion rate decreases in the cubic phase, the blue shift becomes more rapid, suggesting more than just temperature-driven thermal expansion. PL data serves as a proxy to the band gap of the material, which arises from how the atomic orbitals overlap to form the band structure. In $CsSnBr_3$, valence band maximum (VBM) is primarily comprised of Sn $5s$ and Br $4p$ orbital overlap and the conduction band minimum (CBM) of Sn $5p$ and Br

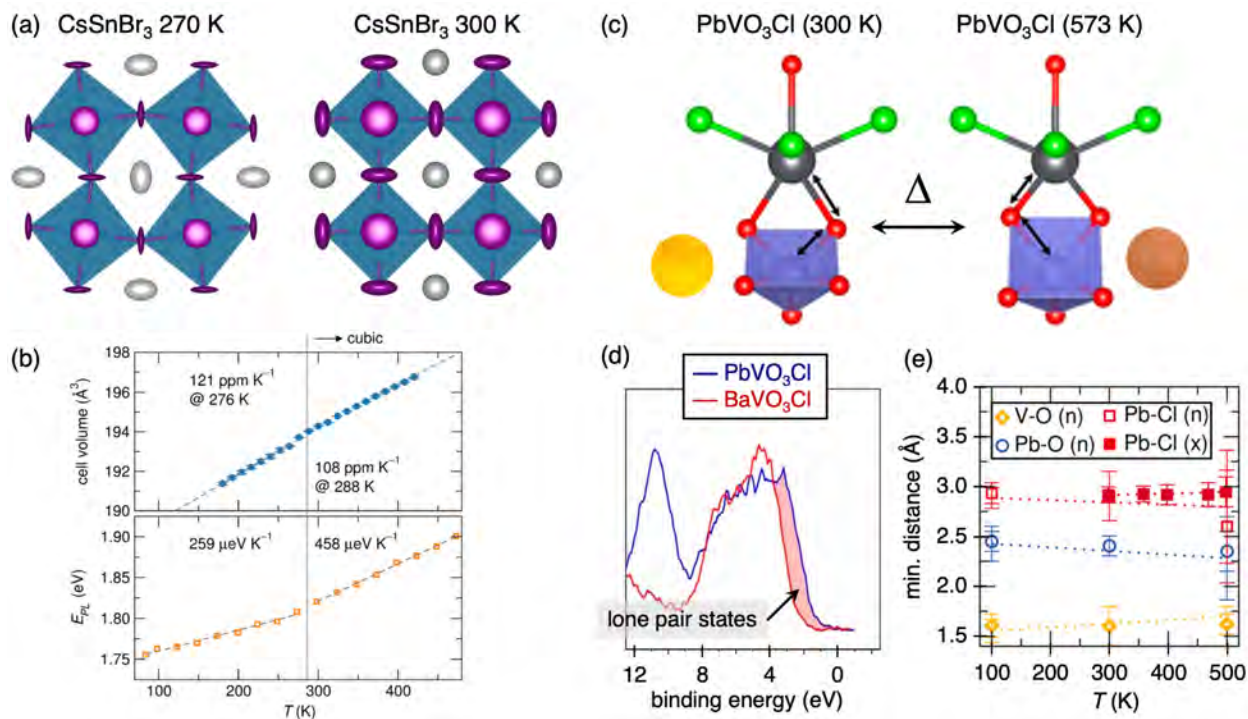


Figure 7: (a) Two crystallographic structures of CsSnBr₃: tetragonal $P4/mbm$ at 270 K and cubic $Pm\bar{3}m$ at 300 K (ADPs for all structures shown at 90% probability). (b) Experimental evolution of unit cell volume and photoluminescence (PL) emission peak energy, E_{PL} , with temperature. (c) Structural changes in PbVO₃Cl and observed color change. (d) Hard X-ray photoemission spectra of PbVO₃Cl and BaVO₃Cl at an incident photon energy of 5.0 keV. (e) V-O, Pb-O, and Pb-Cl distances with temperature from the analysis of neutron (n, NOMAD, Oak Ridge National Laboratory) and X-ray (x, 11-ID-B, Argonne National Laboratory) PDF data. Adapted with permission from ref. ¹ (Copyright 2016 American Chemical Society) and ref. ⁶³ (Copyright 2020 American Chemical Society).

4*p* orbitals. Calculations of the electronic band gap as a function of temperature revealed that this additional rate increase is explained by the dynamic stereochemical activity of lone pairs associated with Sn²⁺. Thermal expansion lengthens the Sn–Br bond, which reduces orbital overlap and results in a simultaneous narrowing of both bands and lowering of the VBM and CBM, which both have antibonding character. This results in a widening of the band gap, which is further enhanced with Sn²⁺ off-centering, accounting for the rate increase in the lone-pair active region of this material. The impact of lone pairs on the properties of inorganic and hybrid halide perovskites of Sn²⁺ and Pb²⁺ has been summarized recently.⁶⁴ The general principles of employing lone pairs as a design element in photovoltaic absorbers has also been examined in a systematic manner.^{65,66}

Another example of the influence of lone pair behavior on optical properties is in the thermochromic material PbVO₃Cl.⁶³ This material exhibits a color change from yellow to red above 573 K (shown in figure 7c), which is not accompanied by a crystallographic phase transition. A combined approach of total scattering, HAXPES, and DFT revealed behavior in PbVO₃Cl that was not present in the *s*⁰ analog BaVO₃Cl (figure 7d). Warming PbVO₃Cl leads to Pb off-centering, which is proposed to be due to lone pair stereochemistry. This material presents a unique opportunity to observe lone pair behavior in a mixed-anion coordination environment. The displacement of Pb results in an anharmonic lattice where the Pb–O bond lengths decrease and the Pb–Cl bond lengths remain unchanged (figure 7e). This follows the expected trends that guide lone pair stereochemistry: there is a stronger hybridization between Pb 6*s*² and O 2*p* states, evidenced by decreasing bond lengths, which, when coupled with an increasing V–O bond length, results in a narrowing of the band gap and a shift from yellow to red.

We have recently demonstrated that disordered lone pair behavior plays a crucial role in the compositionally-driven insulator-to-metal transition in the pyrochlore solid solution (Pr_{1–*x*}Bi_{*x*})₂Ru₂O₇.⁴ This work was motivated by a simple model that increasing the size of the *A*-site cation increases the Ru–O–Ru bond angle, allowing for greater Ru 4*d*–O 2*p*

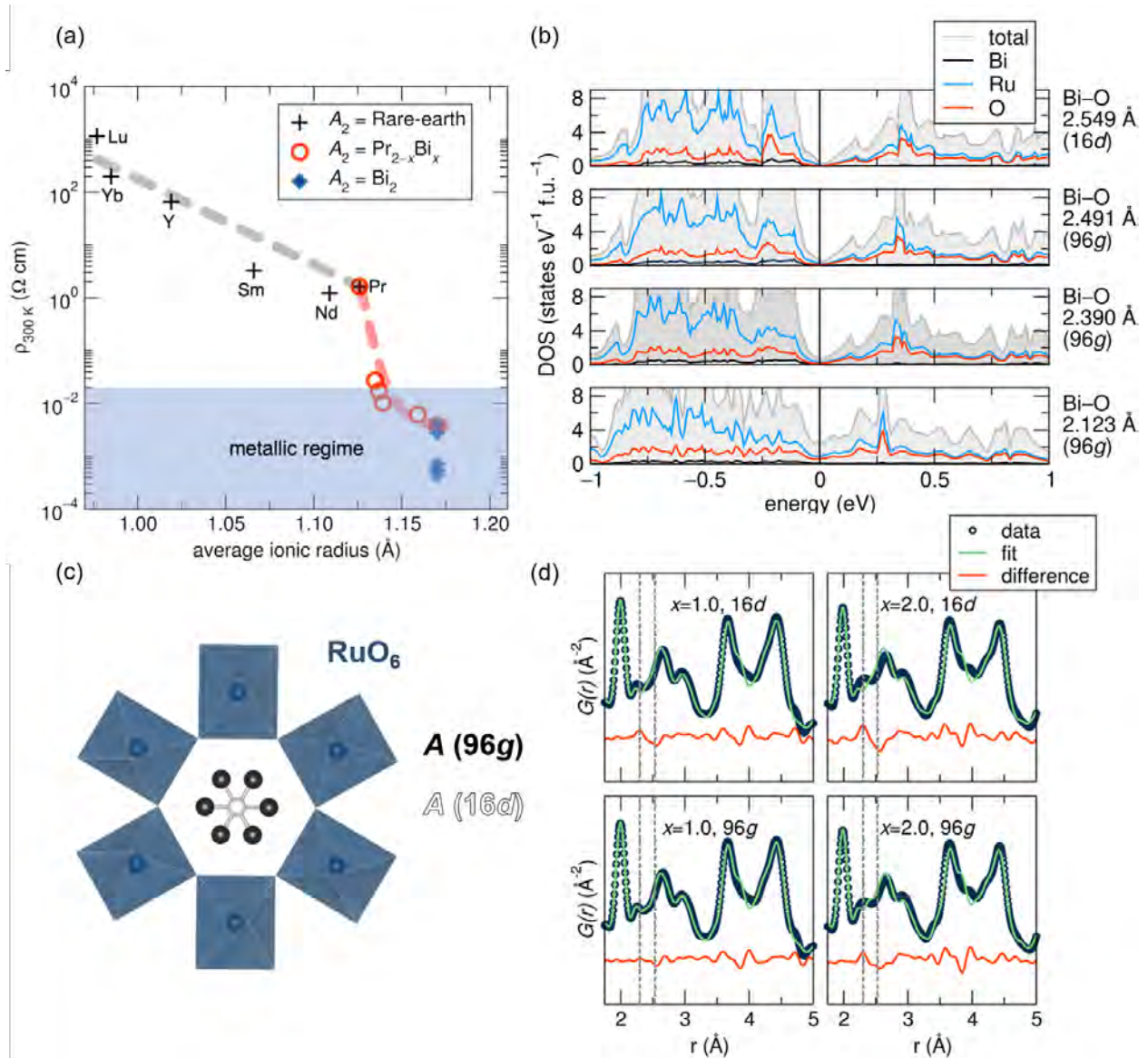


Figure 8: (a) Room temperature resistivity $\rho(300\text{ K})$ as a function of the average A -site ionic radii for the series $(\text{Pr}_{1-x}\text{Bi}_x)_2\text{Ru}_2\text{O}_7$ ($x = 0.0, 0.1, 0.5, \text{ and } 1.0$), shown in open circles, illustrates a cross-over from insulating to metallic conductivity between $x = 0.1$ and $x = 1.0$. (b) Total and projected density of states (DOS) for stoichiometric $\text{Bi}_2\text{Ru}_2\text{O}_7$ as a function of the Bi^{3+} displacements from the $16d$ to $96g$ Wyckoff site. The energies are referenced to the Fermi at 0 eV (vertical line). (d) Fits of the neutron PDF (NPDF, Los Alamos National Laboratory) against the crystallographic structure with the A -site cation in the ideal $16d$ Wyckoff site at $(0.5, 0.5, 0.5)$ and with the A -site cation displaced into the $96g$ Wyckoff site at (x, x, z) [shown in (c)]. For both the $x = 0.5$ and $x = 1.0$ samples the data is better described by the $96g$ model. Dashed lines indicate A -O bond lengths when the A -site cation is placed in the ideal $16d$ position. Adapted with permission from ref. ⁴ Copyright 2019 American Physical Society.

overlap. We hypothesized that this size-dependent structural change drives the system from insulating to metallic behavior, as is observed across the series of Bi-substituted rare-earth pyrochlores (figure 8a). In this panel, room temperature electrical resistivity data is compared from several literature sources on $A_2Ru_2O_7$ pyrochlores⁶⁷⁻⁷² and displays a non-monotonic decrease in resistivity with increasing average A -cation size, particularly when Bi^{3+} is alloyed into the A -site. The Pr-Bi solid solution was probed through neutron total scattering techniques coupled with DFT calculations. Lone-pair driven Bi^{3+} off-centering in various $Bi_2M_2O_7$ pyrochlores was previously established in our earlier work on related materials,⁵¹⁻⁵³ and this work further clarified the role of lone pairs across a solid solution.

Neutron PDF analysis (figure 8d) revealed that even a small substitution of Bi^{3+} on the pyrochlore A site leads to a shift from the ideal $16d$ Wyckoff site to the off-centered $96g$ site (figure 8c), enhancing the average effective size of the A -site cation. This supports the hypothesis that the insulator-to-metal transition is driven by an increasing effective A -site radius. However, DFT calculations suggested this effect was more than just merely due to the increased size, and the off-centered Bi^{3+} had observable effects on the Ru and O contributions to the density of states (DOS, figure 8b). In unsubstituted $Pr_2Ru_2O_7$, electron correlation results in insulating behavior in the material. When Bi occupies the ideal $16d$ site in $Bi_2Ru_2O_7$, the DOS indicates hybridization between Bi $6p$ and Ru $4d_{t2g}$ orbitals, which mediates Ru $4d$ and O $2p$ overlap and results in strong Ru–O bonds. The DOS reveals that this hybridization also gives rise to a pseudogap at E_F (top panel of figure 8b), with $Bi_2Ru_2O_7$ appearing to be semimetallic. When the Bi atom displaces into the $96g$ position, the Ru–O bonding interaction is weakened and the pseudogap closes (middle and bottom panels of figure 8b), which in turn drives metallic behavior. This combination of primary (electronic) and secondary (size) effects suggests that the role of stereochemically active lone pairs can go beyond steric considerations, offering a new route for the manipulation of functional materials through lone pair substitution.

5 Conclusion and Outlook

This Account has described a few vignettes, from the perspective of the authors, of the excitement associated with lone pairs being employed as a design element in functional, extended crystalline materials. It would be evident to the reader that only a rather small corner of vast space of lone-pair associated functionality has been discussed. In addition to the more transition functionality that lone pairs have been associated with, the prospects for lone pairs to be employed in the develop functionality in emerging materials classes such as topological insulators, Dirac, and Weyl materials⁷³ is an emerging area of research that promises the continued relevance of this simple and historic electronic structural motif in the future of materials chemistry.

Acknowledgement

We thank Sam Teicher for the DFT calculation and visualization employed in displaying the lone pairs in Pb^{2+} in $\alpha\text{-PbO}$. G. L. gratefully acknowledges support for this work from Bates College, and from the National Science Foundation through DMR 1904980. R. S. gratefully acknowledges support for this work from the U.S. Department of Energy, Office of Science, Basic Energy Sciences through DE-SC-0012541.

6 Biographical Information

Geneva Laurita completed a B.S. in Chemistry at the University of Northern Colorado in 2010, and Ph.D. in Chemistry at the Oregon State University in 2014. Following postdoctoral research at the University of California, Santa Barbara, Geneva started as an Assistant Professor of Chemistry and Biochemistry at Bates College in 2017. Geneva's research focuses on understanding structure—property relationships of oxide compounds with an emphasis on neutron and synchrotron X-ray total scattering techniques.

Ram Seshadri completed a B.Sc. (Hons) in Chemistry from Delhi University in 1989, and a PhD. in Solid State Chemistry at the Indian Institute of Science in 2005. Following postdoctoral research in the Laboratoire CRISMAT in Caen and the Johannes Gutenberg-Universität in Mainz, Ram started as an Assistant Professor at the Indian Institute of Science in 1999, and moved in 2002 to the University of California, Santa Barbara. Ram's research and teaching focus on structure-property relations in functional inorganic and hybrid materials.

References

- 1 Fabini, D. H.; Laurita, G.; Bechtel, J. S.; Stoumpos, C. C.; Evans, H. A.; Kontos, A. G.; Raptis, Y. S.; Falaras, P.; Van der Ven, A.; Kanatzidis, M. G.; Seshadri, R. Dynamic Stereochemical Activity of the Sn²⁺ Lone Pair in Perovskite CsSnBr₃. *J. Amer. Chem. Soc.* **2016**, *138*, 11820–11832, PMID: 27583813.
- 2 Laurita, G.; Fabini, D. H.; Stoumpos, C. C.; Kanatzidis, M. G.; Seshadri, R. Chemical Tuning of Dynamic Cation Off-Centering in the Cubic Phases of Hybrid Tin and Lead Halide Perovskites. *Chem. Sci.* **2017**, *8*, 5628–5635.
- 3 Laurita, G.; Page, K.; Suzuki, S.; Seshadri, R. Average and local structure of the Pb-free ferroelectric perovskites (Sr,Sn)TiO₃ and (Ba,Ca,Sn)TiO₃. *Phys. Rev. B* **2015**, *92*, 214109.
- 4 Laurita, G.; Puggioni, D.; Hickox-Young, D.; Rondinelli, J. M.; Gaultois, M. W.; Page, K.; Lamontagne, L. K.; Seshadri, R. Uncorrelated Bi Off-Centering and the Insulator-to-Metal Transition in Ruthenium A₂Ru₂O₇ pyrochlores. *Phys. Rev. Mater* **2019**, *3*, 095003.
- 5 Thomson, J. J. XL. Cathode Rays. *Philos. Mag.* **1897**, *44*, 293–316.
- 6 Lewis, G. N. The Atom and the Molecule. *J. Am. Chem. Soc.* **1916**, *38*, 762–785.
- 7 Jensen, W. B. Abegg, Lewis, Langmuir, and the Octet Rule. *J. Chem. Educ.* **1984**, *61*, 191–200.
- 8 Sidgwick, N. V.; Powell, H. M. Bakerian Lecture: Stereochemical Types and Valency Groups. *Proc. R. Soc. A.* **1940**, *176*, 153–180.
- 9 Gillespie, R.; Nyholm, R. Inorganic Stereochemistry. *Quart. Rev. Chem. Soc.* **1957**, *11*, 339–380.
- 10 Momma, K.; Izumi, F. VESTA: A Three-Dimensional Visualization System for Electronic and Structural Analysis. *J. Appl. Crystallogr.* **2008**, *41*, 653–658.

- 11 Kuhs, W.; Finney, J.; Vettier, C.; Bliss, D. Structure and Hydrogen Ordering in Ices VI, VII, and VIII by Neutron Powder Diffraction. *J. Chem. Phys.* **1984**, *81*, 3612–3623.
- 12 Lynden-Bell, R. M.; Morris, S. C.; Barrow, J. D.; Finney, J. L.; Harper, C. *Water and Life: the Unique Properties of H₂O*; CRC Press, 2019.
- 13 Hewat, A.; Riekel, C. The Crystal Structure of Deuteroammonia Between 2 and 180 K by Neutron powder Profile Refinement. *Acta Crystallogr. A* **1979**, *35*, 569–571.
- 14 Gordon, J. P.; Zeiger, H. J.; Townes, C. H. The Maser — New Type of Microwave Amplifier, Frequency Standard, and Spectrometer. *Phys. Rev.* **1955**, *99*, 1264–1274.
- 15 Le Page, Y.; Donnay, G. Refinement of the Crystal Structure of Low-Quartz. *Acta Crystallogr. B* **1976**, *32*, 2456–2459.
- 16 Orgel, L. The Stereochemistry of B Subgroup Metals. Part II. The Inert Pair. *J. Chem. Soc.* **1959**, 3815–3819.
- 17 Walsh, A.; Payne, D. J.; Egdell, R. G.; Watson, G. W. Stereochemistry of Post-Transition Metal Oxides: Revision of the Classical Lone Pair Model. *Chem. Soc. Rev.* **2011**, *40*, 4455–4463.
- 18 Bersuker, I. B. Pseudo-Jahn–Teller Effect – A Two-State Paradigm in Formation, Deformation, and Transformation of Molecular Systems and Solids. *Chem. Rev.* **2013**, *113*, 1351–1390.
- 19 Andersson, S.; Åström, A.; Galy, J.; Meunier, G. Simple Calculations of Bond Lengths and Bond Angles in Certain Oxides, Fluorides or Oxide Fluorides of Sb³⁺, Te⁴⁺ and Pb²⁺. *J. Solid State Chem.* **1973**, *6*, 187–190.
- 20 Galy, J.; Meunier, G.; Andersson, S.; Åström, A. Stéréochimie des Éléments Comportant des Paires Non Liées: Ge (II), As (III), Se (IV), Br (V), Sn (II), Sb (III), Te (IV), I (V), Xe

- (VI), Tl (I), Pb (II), et Bi (III) (Oxydes, Fluorures et Oxyfluorures). *J. Solid State Chem.* **1975**, *13*, 142–159.
- 21 Hyde, B.; Andersson, S. *Inorganic Crystal Structures*; Wiley: New York, 1989.
- 22 Andersson, S. On the Stereochemistry of Valence Bonds and the Structures of XeO_3 , XeF_4 and XeF_2 . *Acta Crystallogr. B* **1979**, *35*, 1321–1324.
- 23 Pyykkö, P.; Desclaux, J. P. Relativity and the Periodic System of Elements. *Acc. Chem. Res.* **1979**, *12*, 276–281.
- 24 Hohenberg, P.; Kohn, W. Inhomogeneous Electron Gas. *Phys. Rev.* **1964**, *136*, B864–871.
- 25 Kohn, W.; Sham, L. J. Self-Consistent Equations Including Exchange and Correlation Effects. *Phys. Rev.* **1965**, *140*, A1133–A1138.
- 26 Becke, A. D.; Edgecombe, K. E. A Simple Measure of Electron Localization in Atomic and Molecular Systems. *J. Chem. Phys.* **1990**, *92*, 5397–5403.
- 27 Silvi, B.; Savin, A. Classification of Chemical Bonds Based on Topological Analysis of Electron Localization Functions. *Nature* **1994**, *371*, 683–686.
- 28 Seshadri, R.; Hill, N. A. Visualizing the Role of Bi 6s “Lone Pairs” in the Off-Center Distortion in Ferromagnetic BiMnO_3 . *Chem. Mater.* **2001**, *13*, 2892–2899.
- 29 Portier, J.; Reau, J.; Matar, S.; Soubeyroux, J.; Hagenmuller, P. Advances on Fluorine Ion Conductors, Basic and Applied Research. *Solid State Ionics* **1983**, *11*, 83–90.
- 30 Wuttig, M.; Lüsebrink, D.; Wamwangi, D.; Welnic, W.; Gilleßen, M.; Dronskowski, R. The Role of Vacancies and Local Distortions in the Design of New Phase-Change Materials. *Nat. Mater.* **2007**, *6*, 122–128.

- 31 Larson, P.; Mahanti, S.; Kanatzidis, M. Electronic Structure and Transport of Bi₂Te₃ and BaBiTe₃. *Phys. Rev. B* **2000**, *61*, 8162.
- 32 Zeier, W. G.; Zevalkink, A.; Gibbs, Z. M.; Hautier, G.; Kanatzidis, M. G.; Snyder, G. J. Thinking Like a Chemist: Intuition in Thermoelectric Materials. *Angew. Chemie* **2016**, *55*, 6826–6841.
- 33 Isaacs, E. B.; Lu, G. M.; Wolverton, C. Inverse Design of Ultralow Lattice Thermal Conductivity Materials via Materials Database Screening of Lone Pair Cation Coordination Environment. *J. Phys. Chem. Lett.* **2020**, *11*, 5577–5583.
- 34 Tung, Y.; Cohen, M. L. Relativistic Band Structure and Electronic Properties of SnTe, GeTe, and PbTe. *Phys. Rev.* **1969**, *180*, 823.
- 35 Fu, L. Topological Crystalline Insulators. *Phys. Rev. Lett.* **2011**, *106*, 106802.
- 36 Tanaka, Y.; Ren, Z.; Sato, T.; Nakayama, K.; Souma, S.; Takahashi, T.; Segawa, K.; Ando, Y. Experimental Realization of a Topological Crystalline Insulator in SnTe. *Nat. Phys.* **2012**, *8*, 800–803.
- 37 Ok, K. M.; Halasyamani, P. S. The Lone-Pair Cation I⁵⁺ in a Hexagonal Tungsten Oxide-Like Framework: Synthesis, Structure, and Second-Harmonic Generating Properties of Cs₂I₄O₁₁. *Angew. Chemie* **2004**, *116*, 5605–5607.
- 38 Halasyamani, P. S. Asymmetric Cation Coordination in Oxide Materials: Influence of Lone-Pair Cations on the Intra-Octahedral Distortion in *d*⁰ Transition Metals. *Chem. Mater.* **2004**, *16*, 3586–3592.
- 39 Bersuker, I. B. *The Jahn-Teller Effect and Vibronic Interactions in Modern Chemistry*; Plenum Press: New York, 1984.

- 40 Lefebvre, I.; Lannoo, M.; Allan, G.; Ibanez, A.; Fourcade, J.; Jumas, J. C.; Beurepaire, E. Electronic Properties of Antimony Chalcogenides. *Phys. Rev. Lett.* **1987**, *59*, 2471–2474.
- 41 Lefebvre, I.; Szymanski, M. A.; Olivier-Fourcade, J.; Jumas, J. C. Electronic Structure of Tin Monochalcogenides from SnO to SnTe. *Phys. Rev. B* **1998**, *58*, 1896–1906.
- 42 Watson, G.; Parker, S. Origin of the Lone Pair of α -PbO from Density Functional Theory Calculations. *J. Phys. Chem. B* **1999**, *103*, 1258–1262.
- 43 Watson, G. W.; Parker, S. C.; Kresse, G. Ab Initio Calculation of the Origin of the Distortion of α -PbO. *Phys. Rev. B* **1999**, *59*, 8481–8486.
- 44 Bent, H. A. An Appraisal of Valence-bond Structures and Hybridization in Compounds of the First-Row Elements. *Chem. Rev.* **1961**, *61*, 275–311.
- 45 Power, P. P. π -Bonding and the Lone Pair Effect in Multiple Bonds Between Heavier Main Group Elements. *Chem. Rev.* **1999**, *99*, 3463–3504.
- 46 Waghmare, U. V.; Spaldin, N. A.; Kandpal, H. C.; Seshadri, R. First-Principles Indicators of Metallicity and Cation Off-Centricity in the IV-VI Rocksalt Chalcogenides of Divalent Ge, Sn, and Pb. *Phys. Rev. B* **2003**, *67*, 125111.
- 47 Woodward, P. M.; Karen, P.; Evans, J. S. O.; Vogt, T. *Solid State Materials Chemistry*; Cambridge University Press: Cambridge, United Kingdom New York, NY, USA, 2021.
- 48 Bozin, E. S.; Malliakas, C. D.; Souvatzis, P.; Proffen, T.; Spaldin, N. A.; Kanatzidis, M. G.; Billinge, S. J. L. Entropically Stabilized Local Dipole Formation in Lead Chalcogenides. *Science* **2010**, *330*, 1660–1663.
- 49 Knox, K. R.; Bozin, E. S.; Malliakas, C. D.; Kanatzidis, M. G.; Billinge, S. J. L. Local Off-Centering Symmetry Breaking in the High-Temperature Regime of SnTe. *Phys. Rev. B* **2014**, *89*, 014102.

- 50 Dmowski, W.; Vakhrushev, S. B.; Jeong, I.-K.; Hehlen, M. P.; Trouw, F.; Egami, T. Local Lattice Dynamics and the Origin of the Relaxor Ferroelectric Behavior. *Phys. Rev. Lett.* **2008**, *100*, 137602.
- 51 Seshadri, R. Lone Pairs in Insulating Pyrochlores: Ice Rules and High- k Behavior. *Solid State Sci.* **2006**, *8*, 259–266.
- 52 Shoemaker, D. P.; Seshadri, R.; Hector, A. L.; Llobet, A.; Proffen, T.; Fennie, C. J. Atomic displacements in the charge ice pyrochlore $\text{Bi}_2\text{Ti}_2\text{O}_6\text{O}'$ studied by neutron total scattering. *Phys. Rev. B* **2010**, *81*, 144113.
- 53 Shoemaker, D. P.; Seshadri, R.; Tachibana, M.; Hector, A. L. Incoherent Bi off-centering in $\text{Bi}_2\text{Ti}_2\text{O}_6\text{O}'$ and $\text{Bi}_2\text{Ru}_2\text{O}_6\text{O}'$: Insulator versus metal. *Phys. Rev. B* **2011**, *84*, 064117.
- 54 Evans, I. R.; Howard, J. A. K.; Evans, J. S. O. α - $\text{Bi}_2\text{Sn}_2\text{O}_7$ – a 176 atom crystal structure from powder diffraction data. *J. Mater. Chem.* **2003**, *13*, 2098–2103.
- 55 Ganne, M.; Tournoux, M. Structure et Anomalie Dielectrique de $\text{Tl}_2\text{Ta}_2\text{O}_6$. *Mater. Res. Bull.* **1975**, *10*, 1313–1317.
- 56 Birchall, T.; Sleight, A. Nonstoichiometric Phases in the Sn–Nb–O and Sn–Ta–O Systems Having Pyrochlore-Related Structures. *J. Solid State Chem.* **1975**, *13*, 118–130.
- 57 Avdeev, M.; Haas, M.; Jorgensen, J.; Cava, R. Static Disorder from Lone-Pair Electrons in $\text{Bi}_{2-x}\text{M}_x\text{Ru}_2\text{O}_{7-y}$ ($M = \text{Cu}, \text{Co}; x = 0, 0.4$) Pyrochlores. *J. Solid State Chem* **2002**, *169*, 24–34.
- 58 Wills, A. S.; Ballou, R.; Lacroix, C. Model of localized highly frustrated ferromagnetism: The kagomé spin ice. *Phys. Rev. B* **2002**, *66*, 144407.
- 59 Melot, B.; Rodriguez, E.; Proffen, T.; Hayward, M.; Seshadri, R. Displacive Disorder in Three High- k Bismuth Oxide Pyrochlores. *Mater. Res. Bull.* **2006**, *41*, 61–966.

- 60 Goldschmidt, V. Die Gesetze der Krystallochemie. *Naturwissenschaften* **1926**, *14*, 477–485.
- 61 Wang, J.; Neaton, J.; Zheng, H.; Nagarajan, V.; Ogale, S.; Liu, B.; Viehland, D.; Vaithyanathan, V.; Schlom, D.; Waghmare, U.; Spaldin, N.; Rabe, K.; Wutting, M.; Ramesh, R. Epitaxial BiFeO₃ Multiferroic Thin Film Heterostructures. *Science* **2003**, *299*, 1719–1722.
- 62 Baettig, P.; Seshadri, R.; Spaldin, N. A. Anti-Polarity in Ideal BiMnO₃. *J. Amer. Chem. Soc.* **2007**, *129*, 9854–9855, PMID: 17658812.
- 63 Dang, U.; Zaheer, W.; Zhou, W.; Kandel, A.; Orr, M.; Schwenz, R. W.; Laurita, G.; Banerjee, S.; Macaluso, R. T. Lattice Anharmonicity of Stereochemically Active Lone Pairs Controls Thermochromic Band Gap Reduction of PbVO₃Cl. *Chem. Mater.* **2020**, *32*, 7404–7412.
- 64 Fabini, D. H.; Seshadri, R.; Kanatzidis, M. G. The Underappreciated Lone Pair in Halide Perovskites Underpins their Unusual Properties. *MRS Bulletin* **2020**, *45*, 467–477.
- 65 Ganose, A. M.; Savory, C. N.; Scanlon, D. O. Beyond Methylammonium Lead Iodide: Prospects for the Emergent Field of *ns*² Containing Solar Absorbers. *Chem. Commun.* **2017**, *53*, 20–44.
- 66 Fabini, D. H.; Koerner, M.; Seshadri, R. Candidate Inorganic Photovoltaic Materials from Electronic Structure-Based Optical Absorption and Charge Transport Proxies. *Chem. Mater.* **2019**, *31*, 1561–1574.
- 67 Gaultois, M. W.; Barton, P. T.; Birkel, C. S.; Misch, L. M.; Rodriguez, E. E.; Stucky, G. D.; Seshadri, R. Structural Disorder, Magnetism, and Electrical and Thermoelectric Properties of Pyrochlore Nd₂Ru₂O₇. *J. Phys.: Condens. Matt.* **2013**, *25*, 186004.

- 68 Yamamoto, T.; Kanno, R.; Takeda, Y.; Yamamoto, O.; Kawamoto, Y.; Takano, M. Crystal Structure and Metal-Semiconductor Transition of the $\text{Bi}_{2-x}\text{Ln}_x\text{Ru}_2\text{O}_7$ Pyrochlores ($\text{Ln} = \text{Pr-Lu}$). *J. Solid State Chem.* **2002**, *109*, 24–34.
- 69 Bouchard, R. J.; Gilson, J. L. A New Family of Bismuth – Precious Metal Pyrochlores. *Mat. Res. Bull.* **1971**, *6*, 669–679.
- 70 Zhou, Y.; Matsubara, I.; Funahashi, R.; Sodeoka, S. Thermoelectric Properties of $\text{Ln}_{2-x}\text{Bi}_x\text{Ru}_2\text{O}_7$ Pyrochlores ($\text{Ln} = \text{Nd}$ and Yb). *Mater. Lett.* **2001**, *51*, 347–350.
- 71 Kanno, R.; Takeda, Y.; Yamamoto, T.; Yamamoto, Y.; Yamamoto, O. Crystal Structure and Electrical Properties of the Pyrochlore Ruthenate $\text{Bi}_{2-x}\text{Y}_x\text{Ru}_2\text{O}_7$. *J. Solid State Chem.* **1993**, *102*, 106–114.
- 72 Yasukawa, M.; Kuniyoshi, S.; Kono, T. Thermoelectric Properties of the $\text{Bi}_{2-x}\text{Y}_x\text{Ru}_2\text{O}_7$ ($x=0-2$) Pyrochlores. *Solid State Comm.* **2003**, *126*, 213–216.
- 73 Khoury, J. F.; Schoop, L. M. Chemical Bonds in Topological Materials. *Trends in Chem.* **2021**, *3*, 700–715.

